Journal of Engineering and Technology for Industrial Applications

ITEGAM-JETIA

Manaus, v.11 n.56, p.287-295. November/December, 2025.
DOI: https://doi.org/10.5935/jetia. v11i56.2759

ISSN ONLINE: 2447-0228

RESEARCH ARTICLE OPEN ACCESS

EARLY FAULT DETECTION OF ROLLING ELEMENT BEARINGS USING WAVELET PACKET ENERGY RATIO (WPER)

Jayprakash.P.Dataniya[1*], Utkarsh.A.Patel[2], Hitesh.K.Patel[3] and Divyang.H.Pandya[4*]

[1] L.D.College of Engineering, Gujarat Technological University Ahmedabad, India.
[2] Government Engineering College, Patan, Gujarat,India
[3]Research Scholar at Kadi Sarva Vishwavidyalaya, Gandhinagar, Gujarat, India
[4]LDRP Institute of Technology & Research, KSV University, Gandhinagar, Gujarat, India

[1]http://orcid.org/0009-0001-2735-0081, [2]https://orcid.org/0000-0003-4720-2147
[3]https://orcid.org/0009-0000-9217-0354, [4]http://orcid.org/0000-0002-1619-6170

Email: * jayprakashdataniya@ldce.ac.in, utkarsh671975@gmail.com, patelpatelhitesh88@gmail.com, veddhrumi@gmail.com

ARTICLE INFO

Article History
Received: September 29, 2025
Revised: November 20, 2025
Accepted: December 1, 2025
Published: December 31, 2025

Keywords:
Deep groove ball bearing, localized defect, reverse biorthogonal wavelet, energy sub band, time-frequency analysis.

ABSTRACT

Early detection of defects in high-speed ball bearings is critical for preventing machinery failures and unplanned downtime. This study introduces a wavelet-packet–energy-based diagnostic method for identifying incipient bearing faults. Five real wavelets were evaluated, and the reverse Biorthogonal 5.5 wavelet was selected as the optimal basis according to the maximum energy-to-Shannon-entropy ratio criterion. Vibration signals from healthy and faulty bearings were acquired and decomposed using Wavelet Packet Decomposition (WPD) into narrow frequency sub-bands. An energy-ratio metric—defined as the energy of the faulty condition relative to the healthy condition for each sub-band—was computed to quantify fault severity. The method was experimentally validated using vibration data collected under localized single-defect conditions, including outer-race, inner-race, and rolling-element faults, at multiple rotational speeds. Results demonstrate that the proposed WPD-based energy-ratio approach offers superior sensitivity and accuracy for early fault detection compared with conventional vibration-analysis techniques.

I. INTRODUCTION

Rolling bearings are vital components in rotating machinery, and their malfunction can significantly degrade system performance. Failures may result from factors such as excessive or unexpected loads, inadequate or improper lubrication, poor handling practices, or ineffective sealing. Even small defects can lower efficiency, while more severe damage may cause costly downtime or even catastrophic machine failure [1]. For this reason, vibration signal analysis has emerged as an essential tool in condition monitoring and fault diagnosis, as it enables early detection of incipient bearing faults by revealing critical information about their operating state.
Localized damage in bearings often begins due to concentrated Hertzian contact stresses arising between the rolling elements and the raceways. When a rolling element strikes such a defect, it generates an impulse that excites the natural resonances of the bearing structure [2], [3], [4]. Consequently, the vibration response of a defective bearing takes the form of an exponentially decaying sinusoid at the structural resonance frequency.

Since the impulse duration is extremely short compared to the interval between successive impacts, its energy spreads across a wide frequency range at very low levels, making it easily obscured by noise. When a rolling element traverses the load zone of a bearing, a degree of slippage inevitably occurs, which prevents the generated impact impulses from being reproduced at precisely the same spatial position in successive cycles when the defect is located on a stationary component, such as the outer race. Conversely, when the defect lies on the inner race or on the rolling elements, its position varies with respect to the bearing's load distribution. Consequently, the vibration response manifests as a sequence of impulses whose amplitudes are amplitude-modulated [5]. The impulses generated by bearing faults exhibit variability in both their timing and amplitude, introducing a degree of randomness into the signal. Consequently, the signal deviates from strict periodicity and is better characterized as non-stationary or cyclostationary. In such scenarios, traditional

analysis methods like the Fast Fourier Transform (FFT), which assume signal stationarity, may not effectively detect these faults. Instead, employing cyclic second-order statistical tools—such as cyclic autocorrelation and cyclic spectral density—proves more suitable for demodulating the signal and extracting fault-related features. Non-stationary signals are commonly analyzed using time–frequency methods such as the Short-Time Fourier Transform (STFT), Wigner–Ville distribution, and Wavelet Transform (WT) [6], [7], [8]. Owing to its multi-resolution capability and lack of cross-term interference, WT has become a preferred tool in fault diagnostics. Variants of WT include the Continuous and Discrete Wavelet Transforms, Wavelet Packet Analysis [9–11], and advanced extensions that incorporate post-processing techniques such as singularity analysis [12], [13]. In [14], a wavelet transform applied to vibration signals successfully identified defects in the inner and outer races separately and also detected combined faults. Similarly, [15] employed wavelet packet analysis with Daubechies-12 wavelets to process vibration data and reveal faults in both bearing races.However, the wavelet transform alone can struggle to uncover subtle features when background noise and overlapping spectral components mask critical signatures at similar scales [16].

This limitation can be mitigated using the Wavelet Packet Transform (WPT). By computing the autocorrelation of the selected detail coefficient with the approximation coefficient at level J, and then performing Fourier analysis on the resulting measure function, WPT enables precise localization of transient features. Although WPT maps provide richer diagnostic information, recent studies increasingly highlight alternative approaches such as the Hilbert transform, Hilbert–Huang transform, and Z-transform [17]. Wavelet Packet Decomposition (WPD) combined with Empirical Mode Decomposition (EMD) has proven particularly effective for extracting fault-related frequency components. Through this method, intrinsic mode functions (IMFs) that contain fault characteristics can be isolated, and the energy moments of these IMFs are used as eigenvectors to efficiently represent failure features. Building on these advances, recent research has used energy moments as a fault index to express failure characteristics. In this paper, the acquired vibration signal is decomposed using WPD to a desired level, and the wavelet packet energy in each frequency sub-band is compared with that of a healthy bearing. This approach enables simultaneous diagnosis of bearing conditions at different rotational speeds and can detect localized faults in rolling-element bearings.

II. WAVELET PACKET TRANSFORM (WPT)

The Wavelet Packet Transform (WPT) is an extension of the conventional Discrete Wavelet Transform (DWT) designed to provide a more detailed time–frequency representation of signals. In the DWT framework, at each decomposition stage only the low-frequency approximation coefficients are further decomposed, while the high-frequency detail coefficients remain untouched. This produces a pyramidal structure in which resolution is higher at lower frequencies. However, this selective decomposition can restrict the ability to capture information spread across the full frequency spectrum [18], [19], [20]. WPT overcomes this limitation by decomposing both approximation and detail coefficients at every level, forming a complete binary tree of sub-bands. After *n* levels of decomposition, WPT generates 2n2^n2n sub-bands, each corresponding to a specific frequency interval of the original signal. This fine partitioning provides greater flexibility for analyzing non-stationary or transient signals that contain useful information in both high- and low-frequency ranges. An important step in applying WPT is reordering the levels of decomposition. In the raw binary-tree structure, nodes are indexed according to their parent–child relationships, which do not necessarily match the natural order of frequency.

For meaningful interpretation—particularly in engineering applications such as vibration analysis—the sub-bands must be arranged sequentially from the lowest to the highest frequency. Reordering assigns frequency ranges to each node based on the sampling frequency and the decomposition depth so that the sub-bands become contiguous partitions of the signal spectrum. For example, at three levels of decomposition with sampling frequency FsF_sFs, the ordered bands are [0–Fs/8],[Fs/8–2Fs/8],…,[7Fs/8–Fs][0–F_s/8], [F_s/8–2F_s/8], \ldots, [7F_s/8–F_s][0–Fs/8],[Fs/8–2Fs/8],…,[7Fs/8–Fs]. This reordered structure is especially useful for feature extraction. In rotating-machinery fault diagnosis, characteristic defect frequencies such as BPFO, BPFI, or ball-spin frequency lie in specific bands. By mapping WPT sub-bands to actual frequency ranges, one can compute features such as sub-band energy, entropy, or statistical moments. These features can then be used as inputs to machine-learning models or statistical classifiers to enable accurate fault detection. In summary, WPT provides a complete and detailed signal decomposition, while reordering aligns the decomposition levels with true frequency bands. In this study, a new frequency-order index ppp was introduced at level 5, as shown in Figure 1.

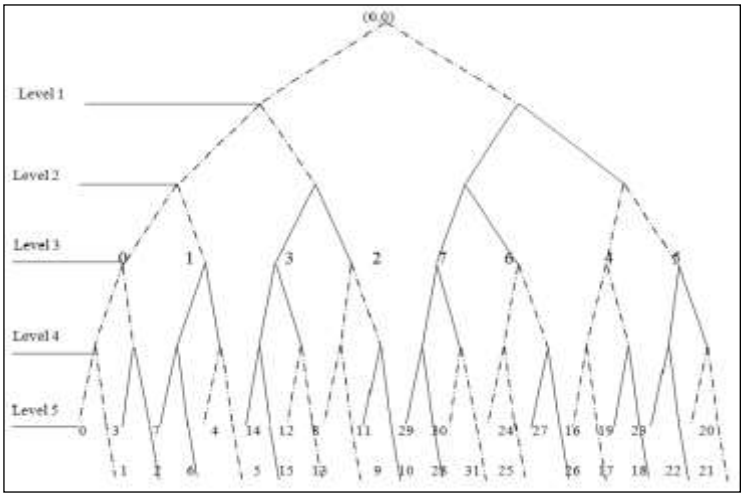

Figure 1: WPT reorders at 5th Level of Decomposition.
Source: Authors, (2025).

III. BALANCED ROTOR WITH VIBRATION ANALYSER SET UP

In this study, experimental trials were performed on a rotor test rig, as shown in Figure 2. The setup comprised a horizontal steel shaft supported by standard 6205 single-row deep-groove ball bearings and driven by a speed-regulated motor. A flexible spring coupling was installed between the motor and rotor shaft to compensate for minor misalignments. The rotor assembly, weighing approximately 2.5 kg, was mounted horizontally and integrated with a data-acquisition unit. Vibration responses were recorded using two bi-axial piezoelectric accelerometers, each with an operating frequency range of 1–30 kHz, a measurement capability of ±500 g (peak), a resolution of 0.005 g, and a resonant frequency of 70 kHz. Data were captured through a four-channel signal analyser with a sampling range of 0.48 Hz to 102.4 kHz. To simulate defective conditions, localized spall faults were introduced on the outer race, inner race, and rolling elements of the bearings. During signal acquisition, a sampling frequency of 2048 Hz and a Hanning window function were employed. Illustrations of the defective bearing cases are provided in Figure 3, and the geometric parameters of the 6205-ball bearing were taken from the manufacturer's catalogue.

Figure 2: Experimental setup,
Source: Authors, (2025).

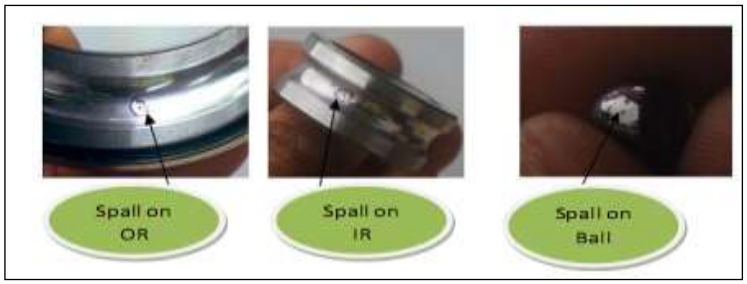

Figure 3: Localized Defect Seeded In Bearing Elements.
Source: Authors, (2025).

Table **1**: Energy to Shannon entropy ratio of real base wavelets under study.

Wavelet Type	Energy to Shannon entropy ratio
Db4	106.28
Db10	95.12
Sym2	82.23
Bior5.5	92.56
Rbio5.5	110.96

Source: Authors, (2025).

III.1 FFT SPECTRUM – OUTCOMES

Figure 4(a)–(d) presents the FFT spectra of all bearing conditions measured in the vertical direction at 3000 rpm. The main frequency components detected are the shaft rotational frequency (ω = 50 Hz), cage frequency (FTF = 19.9 Hz), outer race ball-pass frequency (BPFO = 179 Hz), inner race ball-pass frequency (BPFI = 271 Hz), and ball spin frequency (BSF = 118 Hz).For the healthy bearing (HB), the response is primarily excited at 2X, which leads to the conclusion of misalignment in the rotor-dynamic setup, with an amplitude of 0.03 m/s² [Figure. 4(a)]. In the case of the outer race defect (ORD), a significant response is observed at BPFO = 179 Hz with an amplitude of 0.31714 m/s² [Figure 4(b)]. For the inner race defect (IRD), no distinct fault-related peaks are observed; the dominant

response occurs at 2X with an amplitude of 0.13134 m/s², again attributed to misalignment [Figure 4(c)]. Similarly, for the ball defect (BD), no major fault-specific peaks are recorded; the main responses appear at 2X with an amplitude of 0.04962 m/s² and a minor peak at BPFO = 179 Hz with an amplitude of 0.00652 m/s² [Figure 4(d)]. Evaluated characteristic frequencies at the speed range were tabulated in Table 2.

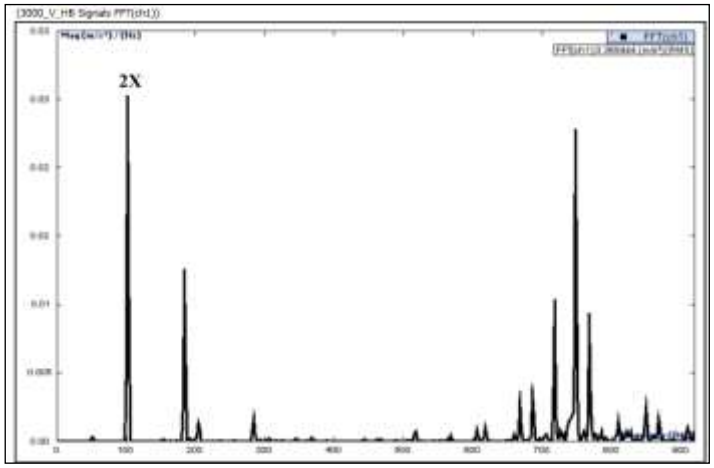

Figure 4(a): FFT of Healthy Bearing at 3000 RPM
Source: Authors, (2025).

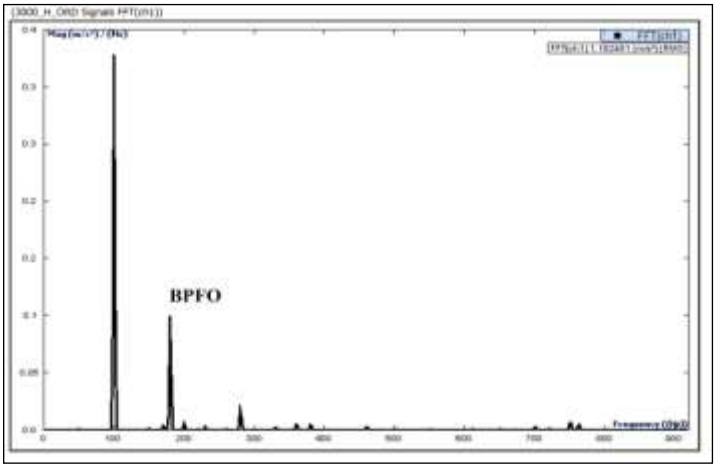

Figure 4(b): FFT of Bearing with Outer Race Defect at 3000 RPM
Source: Authors, (2025).

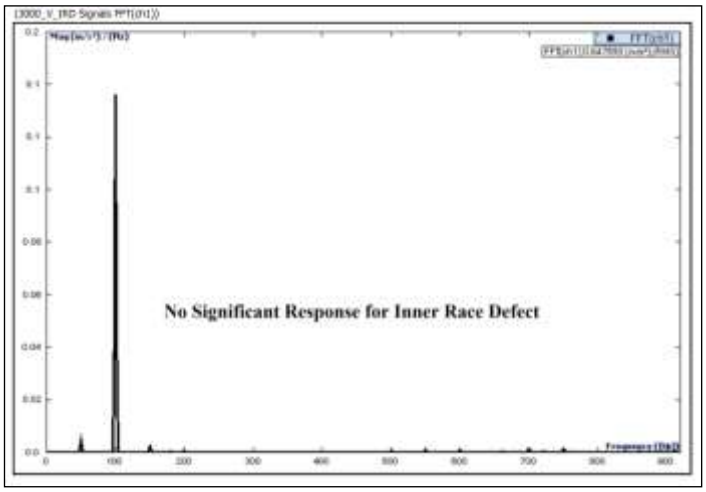

Figure 4(c): FFT of Bearing with Inner Race Defect at 3000 RPM
Source: Authors, (2025).

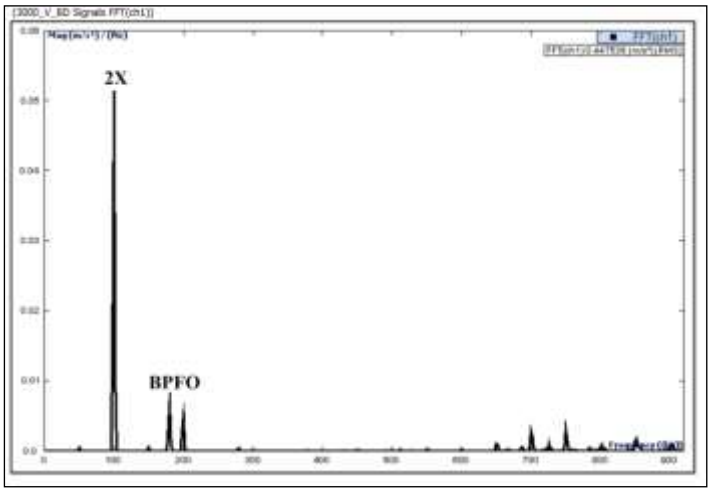

Figure 4(d): FFT of Bearing with Ball defect at 3000 RPM
Source: Authors, (2025).

Table 2: Characteristic Defect frequencies at speed range (1000-6000 RPM).

Speed(RPM)	ω_{inner} (Hz)	ω_{cage} (Hz)	ω_{bpfo} (Hz)	ω_{bpfi} (Hz)	ω_{bsf} (Hz)
1000	16.7	6.64	59.8	90.2	39.3
2000	33.3	13.3	120	180	78.6
3000	50	19.9	179	271	118
4000	66.7	26.6	239	361	157
5000	83.3	33.2	299	451	196
6000	100	39.8	359	541	236

Source: Authors, (2025).

III.2 WPT SPECTRUM – OUTCOMES

The wavelet packet transform (WPT) energy spectra obtained for different bearing conditions in the vertical direction at 3000 rpm are presented in Figure 5(a)–(d). In this approach, the detail coefficients generated by WPT are autocorrelated with the approximate coefficients, and the derived measure is subjected to Fourier transformation to produce the WPT energy spectrum—commonly referred to as the FFT spectrum of WPT. Here, the horizontal axis represents the normalized frequency with respect to the sampling frequency, while the vertical axis indicates the corresponding energy amplitude. This post-spectral method provides improved resolution for detecting transient events. For the healthy bearing (HB), the spectrum shows a dominant peak at a normalized frequency of 0.05 (≈102.4 Hz), which corresponds to the second-order misalignment frequency (2X). A secondary response is observed at 0.08984 (≈185 Hz) with an amplitude of 4.45×10^4 [Figure 5(a)].

In the case of the outer race defect (ORD), a strong excitation appears at the ball-pass frequency of the outer race (BPFO = 0.08789, ≈180 Hz) with an amplitude of 5.339×10^4 [Figure 5(b)]. For the inner race defect (IRD), the most prominent feature is detected at 0.5(BPFI + FTF) = 0.07324 (≈150 Hz), showing an amplitude of 8.6×10^3 [Figure 5(c)]. Finally, for the ball defect (BD), fault-specific spectral lines are not clearly visible. Instead, the main responses occur at 0.05 (≈102.4 Hz) with an amplitude of 10.89×10^4, and at BPFO (≈179 Hz), which is consistent with the trends observed in the conventional FFT spectrum [Figure 5(d)].

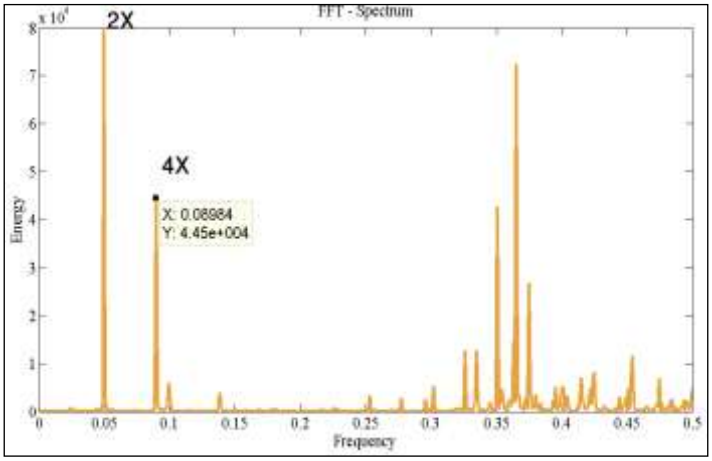

Figure 5(a): WPT energy-spectrum for Healthy Bearing at 3000 RPM.
Source: Authors, (2025).

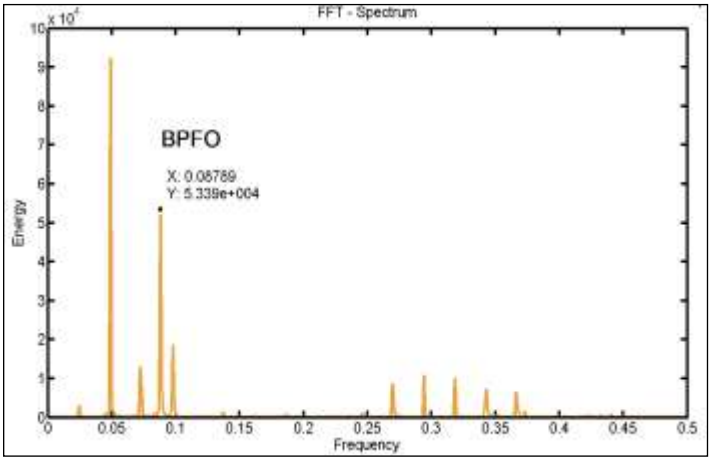

Figure 5(b): WPT energy-spectrum for Bearing with Outer Race Defect at 3000 RPM.
Source: Authors, (2025).

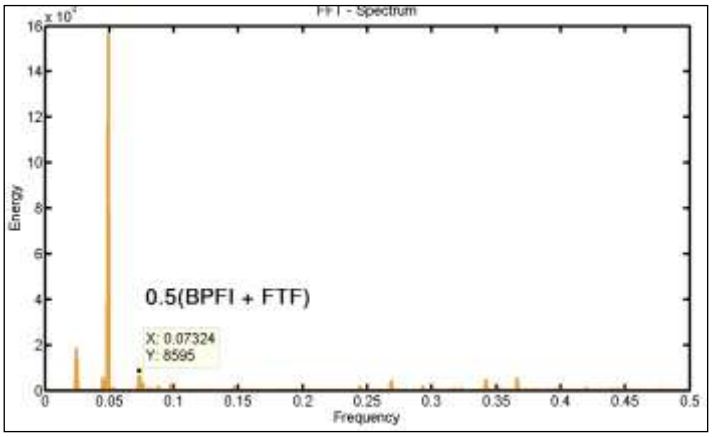

Figure 5(c) WPT energy-spectrum for Bearing with Inner Race Defect at 3000 RPM.
Source: Authors, (2025).

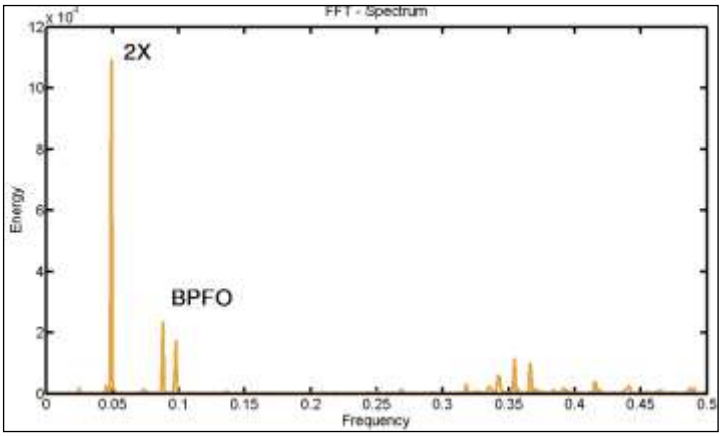

Figure 5(d) WPT energy-spectrum for Bearing with Ball Defect at 3000 RPM.
Source: Authors, (2025).

III.3 DIAGNOSIS WITH WAVELET PACKET ENERGY

Over the past few decades, the wavelet packet transform (WPT) has evolved into a powerful tool for vibration-signal analysis, supported by a wide range of base wavelets. The MATLAB library alone provides 13 different wavelet families [21]. Selecting an appropriate base wavelet is a key step in the diagnostic procedure because it directly affects the accuracy and reliability of fault-detection results. Previous studies have addressed this challenge using qualitative or quantitative selection strategies. In the present work, a quantitative criterion based on the maximum energy-to-Shannon-entropy ratio is adopted to identify the most suitable wavelet for bearing-fault diagnosis. Shannon entropy measures signal disorder and provides insight into the system's dynamical behavior [22]. When the energy probability distribution across decomposition levels approaches uniformity, the corresponding entropy value is near zero or remains very small. Consequently, the optimal wavelet is the one that maximizes extracted signal energy while simultaneously minimizing the Shannon entropy of the autocorrelated WPT coefficients.

In other words, the most effective wavelet for bearing-condition monitoring yields the highest energy-to-entropy ratio. In this study, the energy-to-entropy ratio was computed for four bearing states: (a) healthy bearing (HB), (b) outer race defect (ORD), (c) inner race defect (IRD), and (d) ball defect (BD), under six rotational speeds ranging from 1000 to 6000 rpm. Each test was repeated five times, and the average ratio at each speed was calculated. The wavelet that produced the maximum cumulative average across all operating conditions was selected as the most suitable candidate. Five real wavelets were evaluated, and the results are summarized in Table 1. Based on this comparative analysis, the reverse Biorthogonal 5.5 (rbio5.5) wavelet was identified as the most effective for analysing bearing-vibration signals [22]. For diagnostic purposes, the ratio of energy coefficients between faulty and healthy bearing conditions at the fifth level of decomposition was used as the fault index. At higher decomposition levels, time resolution decreases and the signal energy becomes concentrated in fewer coefficients; however, for transient-signal analysis, decomposition up to the fifth level is effective. In this work, raw signals were decomposed to the fifth level, and the corresponding coefficients for healthy and faulty bearings were denoted

Cj,phC_{j,ph}Cj,ph and Cj,pfC_{j,pf}Cj,pf, respectively. Energy vectors corresponding to these coefficients were computed, and the energy-ratio vector for each sub-band frequency was plotted, as illustrated in Figure. 6(a), Figure. 7(a), and Figure. 8(a) for the ORD, IRD, and BD conditions, respectively. Coefficients from the first nodes were omitted because they contained noisy low frequencies arising from imbalance, misalignment, mechanical looseness, and similar effects.

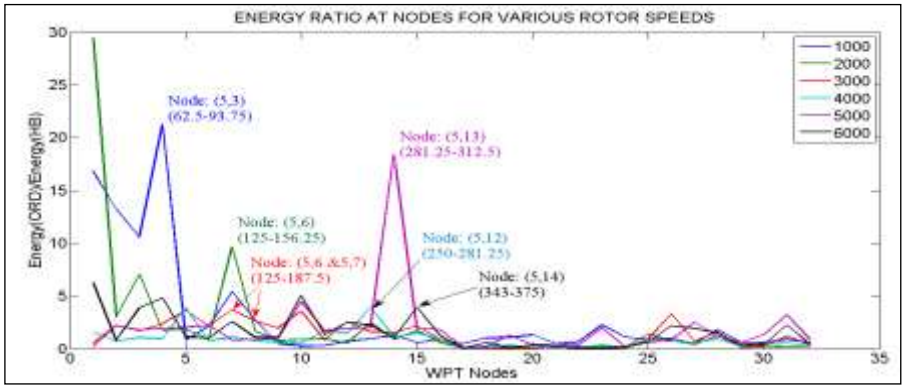

Figure 6(a) Energy ratio (ORD/HB) v/s WPT Nodes at Different speed.
Source: Authors, (2025).

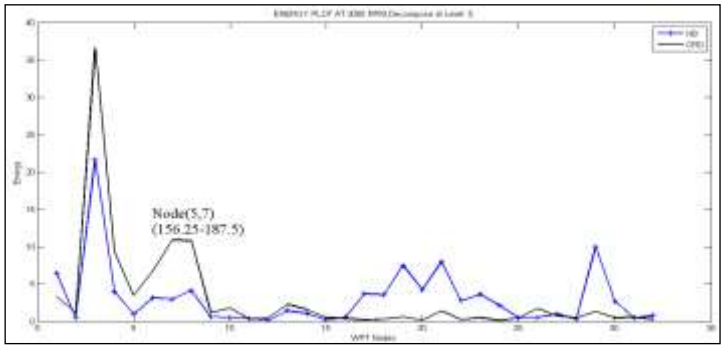

Figure 6(b): Energy v/s WPT Nodes for HB & ORD bearing at 3000 RPM.
Source: Authors, (2025).

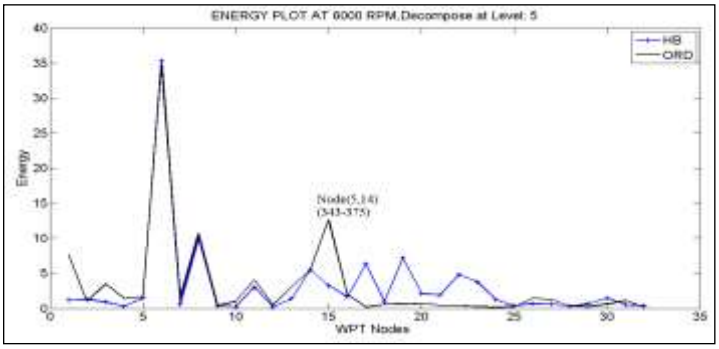

Figure 6(c): Energy v/s WPT Nodes for HB & ORD bearing at 6000 RPM.
Source: Authors, (2025).

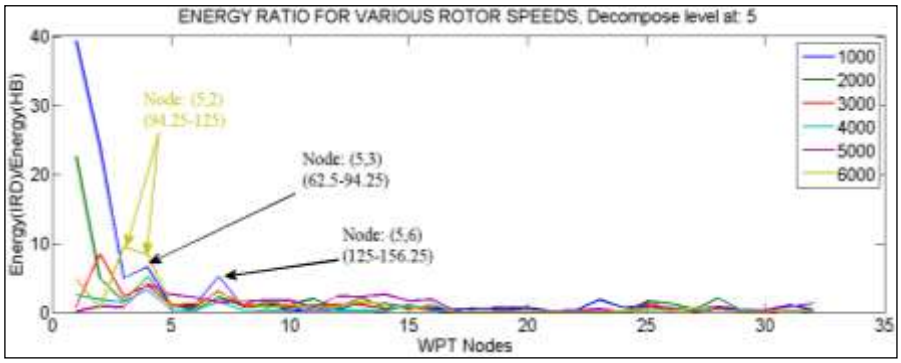

Figure 7(a): Energy ratio (IRD/HB) v/s WPT Nodes at Different speed.
Source: Authors, (2025).

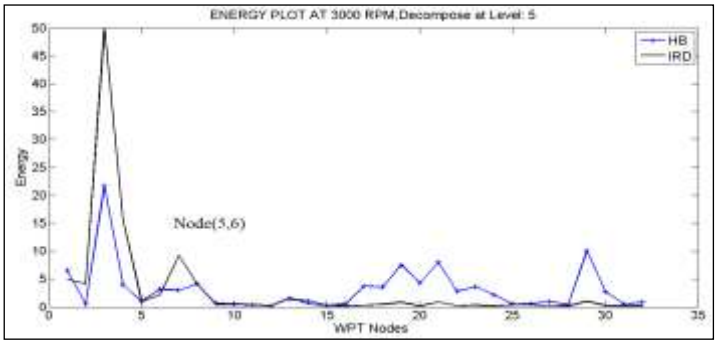

Figure 7(b): Energy v/s WPT Nodes for HB & IRD bearing at 3000 RPM
Source: Authors, (2025).

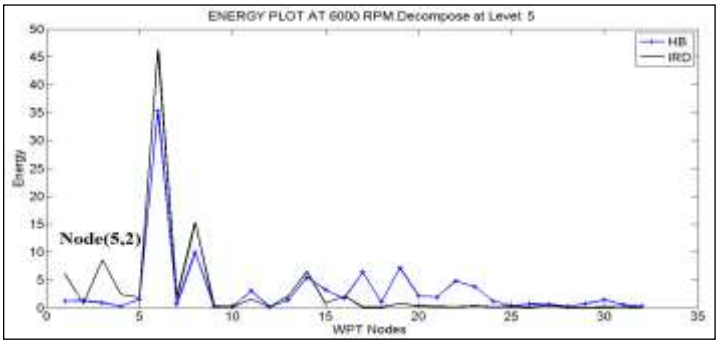

Figure 7 (c) Energy v/s WPT Nodes for HB & IRD bearing at 6000 RPM
Source: Authors, (2025).

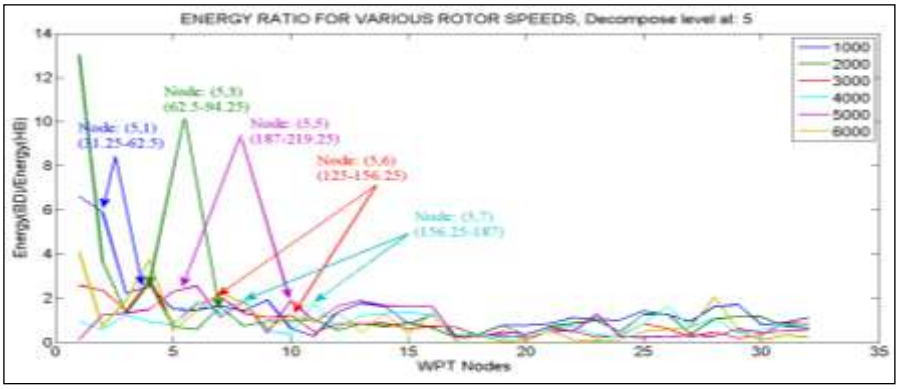

Figure 8(a): Energy ratio (BD/HB) v/s WPT Nodes at Different speed.
Source: Authors, (2025).

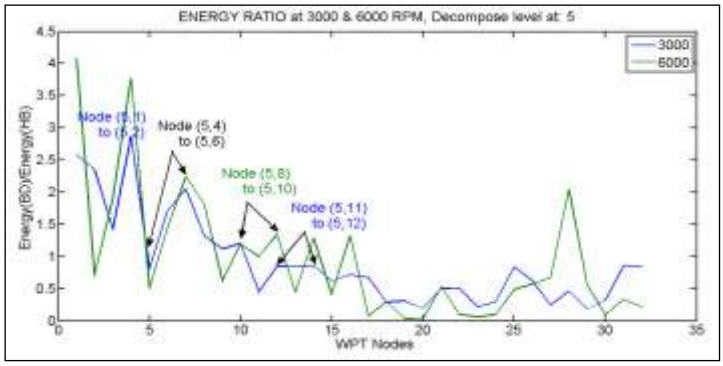

Figure 8(b): Energy ratio (BD/HB) v/s WPT Nodes at 3000 & 6000 RPM.
Source: Authors, (2025).

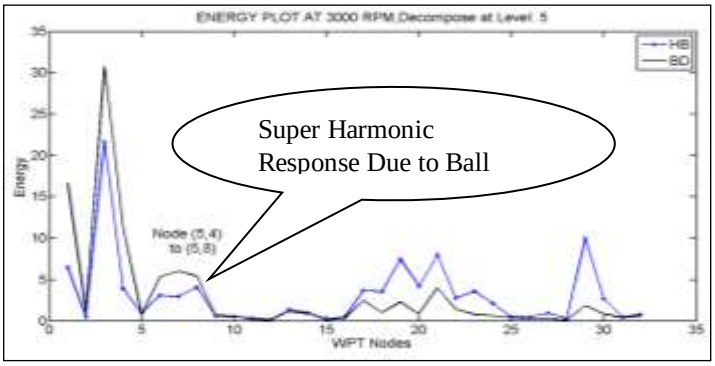

Figure 8(c): Energy v/s WPT Nodes for HB & BD bearing at 3000 RPM
Source: Authors, (2025).

Table 3: Frequency range at excited WPT node.

Node	Frequency Sub band (Hz)	Node	Frequency Sub band (Hz)	Node	Frequency Sub band (Hz)
0	0-31.25	4	218.75-250	9	468.75-500
1	31.25-62.5	5	187.5-218.75	10	375-406.25
2	93.75-125	6	125-156.25	12	250-281.25
3	62.5-93.75	7	156.25-187.5	13	281.25-312.5

Source: Authors, (2025).

IV. RESULTS AND DISCUSSION

Outer Race Defect (ORD) : Figure 6(a) shows the energy ratio of bearings with outer-race defects compared with healthy bearings across all WPT nodes for speeds from 1000 to 6000 rpm. The characteristic defect frequencies for this speed range are listed in Table 3. Clear excitations are observed at node (5,3), node (5,6), between nodes (5,6) and (5,7), node (5,12), and node (5,14) for speeds of 1000, 2000, 3000, 4000, 5000, and 6000 rpm, respectively. For detailed analysis at 3000 and 6000 rpm, energy versus WPT node plots are provided in Fig. 6(b)–(c). Figure 6(b) highlights significant energy separation at node (5,7), indicating robust energy distribution in adjacent nodes and enabling clear diagnosis of an outer-race defect. Similarly, Fig. 6(c) shows strong energy concentration at nodes (5,3) and (5,14); the amplitude difference at node (5,14) confirms the presence of a spall. Although node (5,6) exhibits maximum energy in all conditions, this is attributed to misalignment, as corroborated by the FFT spectrum.

Inner Race Defect (IRD): Figure 7(a) presents the energy ratio for bearings with inner-race defects versus healthy bearings across all WPT nodes for speeds from 1000 to 6000 rpm. Distinct excitations appear at nodes (5,3) and (5,6) throughout the speed range. At 6000 rpm, a flat peak occurs between nodes (5,2) and (5,3). These responses exhibit a subharmonic pattern: at 1000 rpm the excitation is harmonic; at 2000 rpm it is ½ ω_{BPFI}; at 3000 and 4000 rpm it is ¼ ω_{BPFI}; and at 5000 and 6000 rpm it is 1/6 ω_{BPFI}. Further analysis at 3000 and 6000 rpm is shown in Fig. 7(b)–(c). Figure 7(b) demonstrates significant energy separation at node (5,6) for 3000 rpm, while Fig. 7(c) highlights a strong response at node (5,2) for 6000 rpm, confirming the subharmonic excitation pattern and facilitating reliable IRD diagnosis.

Ball Defect (BD): Figure 8(a) illustrates the energy ratio of bearings with a ball defect versus healthy bearings for speeds from 1000 to 6000 rpm. Unlike the ORD and IRD cases, no single node shows a dominant excitation; instead, adjacent nodes collectively form a diagnostic pattern. Across the speed range, responses appear as a flat, inclined trend within the superharmonic frequency bands. Energy disturbances are observed at nodes (5,1)–(5,2), (5,3), (5,4)–(5,5), (5,5)–(5,6), (5,6)–(5,7), (5,8)–(5,10), and (5,9)–(5,10). Superharmonic excitations are clearly marked with arrows in Fig. 8(a) at nodes (5,2)–(5,3), (5,5)–(5,6), (5,10)–(5,11), (5,4)–(5,5), (5,9)–(5,10), and (5,8)–(5,10). Figures 8(b) and 8(c) provide a closer view of the energy distribution at 3000 and 6000 rpm, which represent challenging conditions for high-speed bearing diagnosis. Figure 8(d) further confirms that, while outer- or inner-race defects produce distinct peaks at specific

nodes, ball defects manifest as gradual energy increases across adjacent nodes. Careful observation of these adjacent nodes is therefore essential for accurate ball-defect detection.

V. CONCLUSION

The Fast Fourier Transform (FFT) is effective for diagnosing outer-race defects but is less capable of detecting inner-race or ball defects. Similarly, a WPT-based energy spectrum with an autocorrelation technique can identify outer- and inner-race defects but fails to reliably detect ball defects. The proposed wavelet packet energy ratio (WPER) method significantly enhances the diagnostic capability of WPT, enabling accurate detection of localized defects on the outer race, inner race, and rolling elements. In all cases, the diagnostic information follows a distinct pattern, making the WPER approach more reliable than conventional methods. Observations show that outer-race defects are excited in sub-bands near harmonic frequencies, inner-race defects in sub-bands near subharmonic frequencies, and ball defects in sub-bands near superharmonic frequencies. The sub-band energy responses corresponding to each bearing condition further confirm the effectiveness of the WPER criterion. Because of its flexibility and computational efficiency, WPT provides a robust framework for vibration-signal analysis. The proposed wavelet-selection criterion adds to this framework by offering a quantitative measure that uniquely characterizes the signal and facilitates early fault diagnosis in rolling-element bearings.

VI. AUTHOR'S CONTRIBUTION

Conceptualization: J.P.Dataniya, U.A.Patel, D.H.Pandya.
Methodology: J.P.Dataniya and D.H.Pandya.
Investigation: J.P.Dataniya and D.H.Pandya.
Discussion of results: J.P.Dataniya, U.A.Patel, D.H.Pandya..
Writing – Original Draft: J.P.Dataniya
Writing – Review and Editing: J.P.Dataniya and D.H.Pandya.
Resources: D.H.Pandya.
Supervision: U.A.Patel and D.H.Pandya.
Approval of the final text: J.P.Dataniya, U.A.Patel, D.H.Pandya.

VII. ACKNOWLEDGMENTS

Authors would like to acknowledge the support received from the **Green KSV Skill Development centre, LDRP-ITR Campus, Gandhinagar** for providing vibration analyser and other tooling require for experimental.

VIII. REFERENCES

[1] Ericsson, S., Grip N., Johansson E., Persson, L.E., Sjöberg, R., & Strömberg J.O. (2005). Towards automatic detection of local bearing defects in rotating machines, Mechanical Systems and Signal Processing, 19, 509–535.

[2] Harris, T.A. and Kotzalas, M.N. (2006). Advanced Concepts of Bearing Technology, Boca Raton, FL, CRC Press.

[3] K. Gupta (2006), Rotor Crack Detection Strategies- A Review, Advances in Vibration Engineering, 5(4), 289-306.

[4] Umang Paramar & Pandya D.H. (2021). Comparison of the supervised machine learning techniques using WPT for the fault diagnosis of cylindrical roller bearing, International Journal of Engineering, Science and Technology, 13 (2), 50-60.

[5] Darji, A., Darji, P.H., & Pandya, D.H. (2019). Fault Diagnosis of Ball Bearing with WPT and Supervised Machine Learning Techniques. In: Tanveer, M., Pachori, R. (eds) Machine Intelligence and Signal Analysis. Advances in Intelligent Systems and Computing, 748. Springer, Singapore. https://doi.org/10.1007/978-981-13-0923-6_25

[6] Kiral, Z., & Karagulle, H. (2009). Simulation and Analysis of Vibration Signals Generated by Rolling Element Bearing with Defects, Tribology International, 36(9), 667–678.

[7] Tandon, N., & Choudhury, A. (1997). An Analytical Model for the Prediction of the Vibration Response of Rolling Element Bearings Due to a Localized Defect, Journal of Sound and Vibration, 205(3), 275–292.

[8] Antoni, J., & Randall, R. B. (2002). Differential Diagnosis of Gear and Bearing Faults, ASME Journal of Vibration and Acoustics, 124, 165–171.

[9] Sun Q & Tang Y (2002). Singularity analysis using continuous wave let transform for bearing fault diagnosis, Mechanical Systems and Signal Processing, 16, 1025–1041.

[10] Eren L & Devaney M J (2004). Bearing damage detection via wavelet packet decomposition of the stator current, IEEE Trans. Instrum. Meas., 53, 431–436.

[11] Wang W, Ismail F & Golnaraghi F. (2004). A neuro-fuzzy approach for gear system monitoring, IEEE Trans. Fuzzy Syst., 12, 710–23.

[12] Wang C & Gao R X (2003). Wavelet transform with spectral post-processing for enhanced feature extraction, IEEE Trans. Instrum. Meas., 52, 1296–1301.

[13] Prabhakar S., Mohanty AR., & Sekhar AS (2002). Application of discrete wavelet transform for detection of ball bearing race faults, Journal of Tribology International, 35 (12), 793–800.

[14] Nikolaou N G & Antoniadis I A (2002). Demodulation of vibration signals generated by defects in rolling element bearings using complex shifted Morlet wavelets, Mechanical Systems and Signal Processing, 16, 677–94.

[15] Cheng J, Yu D & Yang Y (2005). Time-energy density analysis based on wavelet transform, NDT&E Int., 38, 569–72.

[16] G.F.Bin, J.J.Gao, X.J.Li, & B.S.Dhillon (2012). Early fault diagnosis of rotating machinery based on wavelet packets — Empirical mode decomposition feature extraction and neural network, Mechanical Systems and Signal Processing, 27, 696–711.

[17] MATLAB R2009a, Release 7.8.0.347, (2009). Wavelet Toolbox, The MathWorks, Inc

[18] Mcfadden, P. D., & Smith, J. D. (1989). Modal for the Vibration Produced by a Single Point Defect in a Rolling Element Bearing, Journal of Sound and Vibration, 96(1), 69–82.

[19] Antoniadis, I., & Glossiotis, G. (2001). Cyclostationary Analysis of Rolling Element Bearing Vibration Signals, Journal of Sound and Vibration , 248(5), 829–845.

[20] Li, L., & Qu, L. (2003). Cyclic Statistics in Rolling Bearing Diagnosis, Journal of Sound and Vibration, 267(2), 253–265.

[21] Ho D, & Randall RB (2000). Optimization of bearing diagnostic techniques using simulated and actual bearing fault signals, Mechanical Systems and Signal Processing , 14 (5), 763-788.

[22] Umang Paramar & Pandya D.H. (2021). Vibration and Acoustics Research Journal, 2 (1), 13-26.